NMR Solution Structure of the Oxidized Form of MerP, a Mercuric Ion Binding Protein Involved in Bacterial Mercuric Ion Resistance[†,‡]

Hong Qian,[§] Lena Sahlman,*[,||] Per-Olof Eriksson,[⊥] Charlotta Hambraeus,[#] Ulf Edlund,[§] and Ingmar Sethson*[,§]

Departments of Organic Chemistry and Biochemistry, Umeå University, S-901 87 Umeå, Sweden, Astra Structural Chemistry Laboratory, S-431 83 Mölndal, Sweden, and University of Southern Stockholm, 141 04, Huddinge, Sweden

Received February 16, 1998; Revised Manuscript Received April 13, 1998

ABSTRACT: Mercuric ions are toxic to living organisms because of their strong affinity for cysteine residues in proteins. Some bacteria have developed a resistance mechanism whereby Hg^{2+} is transported into the cytoplasm and reduced to Hg^0. One of the proteins involved in the transport of mercuric ion is the periplasmic binding protein MerP, which can exist both as oxidized (disulfide) and as reduced (dithiol) forms. Only the reduced form with Cys-17 and Cys-14 residues as free thiols is a potent receptor for mercuric ion. In this work the solution structure of the oxidized form of MerP has been determined by multidimensional NMR spectroscopy and compared to the NMR structures of the previously published structures of the reduced and mercury-bound forms of MerP. The mercury-bound and oxidized forms have similar tertiary structures, whereas in the reduced form there is a large rearrangement of the mercuric ion binding loop and the nearby loop comprising residues 38−41. The structural arrangement of the latter loop seems to be important for the stabilization of the surface location of the cysteine-containing loop. In the reduced form at low pH the cysteine-containing loop adopts a conformation similar to what is observed in the oxidized and mercury-bound forms. The oxidized form also differs with respect to the other two forms in the relative positions of some of the α-helices and β-strands. Structural differences between the oxidized and reduced forms may help explain why the reduced form is stable in the periplasm, which is considered to be an oxidizing environment.

Mercuric ions are toxic to living organisms because of their strong affinity for thiols, such as cysteine residues in proteins. Some bacteria have developed resistance to mercuric ion via reduction of Hg^{2+} to Hg^0, which is less toxic and volatilized from the environment of the cell. While Hg^{2+} is reduced in the cytoplasm by MerA, these bacteria also express MerP, a periplasmic binding protein, as well as the membrane proteins MerT and/or MerC, all believed to be involved in the transport of Hg^{2+} into the cytoplasm. Although MerP is a periplasmic binding protein, transport of mercuric ion shows few similarities with other known periplasmic binding protein-dependent transport systems, e.g., those of maltose or histidine (*1*).

MerP has 72 amino acid residues after cleavage of the amino-terminal signal sequence. These include two cysteine residues, Cys-14 and Cys-17, both of which are necessary for specific binding of Hg^{2+} in the presence of external thiols (*2*, *3*). It is only the dithiol form of the protein that can bind mercuric ion; the oxidized form, with a disulfide bridge, is incapable of Hg^{2+} binding in the presence of external thiols (*2*). Although the reduced form of MerP appears to predominate in the periplasmic environment, the periplasm is generally considered to be an oxidizing medium and some oxidized MerP can also be detected (Powlowski and Sahlman, personal communication).

The secondary structure and global fold of oxidized MerP have previously been determined using NMR[1] spectroscopy (*4*): there are four antiparallel β-sheets, and two major α-helices, forming a so-called open-face β-sheet sandwich (*5*). The two cysteines are located on a loop between the first β-strand and the first α-helix. This structure is in marked contrast to those of 12 other periplasmic binding proteins, which are generally 26−60 kDa in size and have two protein domains which form a deep cleft where the ligand is engulfed by the two domains (*6*).

The solution structures of reduced MerP and MerP with bound Hg^{2+} have recently been published (*7*). The solution structures of these forms agree with the secondary structure and global fold of oxidized MerP (*4*). We have now determined the three-dimensional solution structure of oxi-

[†] This work was supported by grants from Magnus Bergwalls stiftelse (to L.S. and P.O.E.) and from the Swedish Natural Science Research Council (to U.E.).

[‡] The structure coordinates have been deposited in the Brookhaven Protein Data Bank (filename 2hqi).

* Corresponding authors. L.S.: (temporary address) c/o J. Powlowski, Department of Chemistry and Biochemistry, Concordia University, 1455 de Maisonneuve Blvd, W., Montreal, Quebec, Canada H3G 1M8. E-mail: Lena.Sahlman@chem.umu.se. I.S.: Department of Organic Chemistry, Umeå University, S-901 87 Umeå, Sweden. Telephone: +46-90-786 6286. Fax: +46-90-138885. E-mail: Ingmar.Sethson@chem.umu.se.

[§] Department of Organic Chemistry, Umeå University.

[||] Department of Biochemistry, Umeå University.

[⊥] Astra Structural Chemistry Laboratory.

[#] University of Southern Stockholm.

[1] Abbreviations: NMR, nuclear magnetic resonance; 1D, one dimensional; 2D, two dimensional; 3D, three dimensional; RMSD, root-mean-square deviations; NOE, nuclear Overhauser effect.

S0006-2960(98)00362-6 CCC: $15.00
Published on Web 06/12/1998

Table 1: Acquisition Parameters for Heteronuclear 3D NMR Experiments on Oxidized MerP

	nucleus			no. of complex points			spectral width (Hz)			
	F_1	F_2	F_3	F_1	F_2	F_3	F_1	F_2	F_3	scans
HNCACB	^{13}C	^{15}N	^{1}H	80	48	512	11000	2200	8000	8
HCCH-TOCSY	^{1}H	^{13}C	^{1}H	256	64	1024	8000	11000	8000	2
^{15}N-edited NOESY-HSQC	^{1}H	^{15}N	^{1}H	140	64	512	8000	2200	8000	4
^{13}C/^{15}N-edited NOESY-HSQC	^{1}H	^{13}C/^{15}N	^{1}H	128	48	512	7000	5000	7000	8

dized MerP in order to conduct a comparison between the different forms of the protein. Comparison of conserved residues in MerP with proteins containing the heavy-metal binding motif GMTCXXC also suggests structural features that may be important for mercuric ion binding.

EXPERIMENTAL PROCEDURES

Preparation of Protein. MerP was purified from *Escherichia coli* BL21(DE3) harboring a previously described plasmid in which *merP* from transposon Tn*21* is expressed from the T7 RNA polymerase promoter (*2*). MerP is expressed with a periplasmic signal sequence of 19 amino acids which is cleaved off when the protein is exported into the periplasmic space during cell growth. For preparation of ^{15}N-labeled or ^{13}C/^{15}N-labeled protein, bacteria expressing MerP were grown in minimal medium containing Na_2HPO_4 (6 g/L), KH_2PO_4 (3 g/L), NaCl (0.5 g/L), ampicillin (100 mg/L), $^{15}NH_4Cl$ (0.5 g/L), $FeSO_4$ (0.01 mM), K_2SO_4 (0.28 mM), $CaCl_2$ (0.5 mM), and $MgCl_2$ (1 mM) and the following vitamins (1 mg/L): thiamine hydrochloride, pyridoxine hydrochloride, sodium pantothenate, riboflavin, and niacin. The medium also contained glucose or ^{13}C-labeled glucose (2 g/L).

Protein samples for NMR measurements were prepared by dissolving the lyophilized protein in a buffer at pH 4.9 containing 50 mM deuterated acetic acid in D_2O/H_2O (10/90 by volume) (*4*). Before lyophilization the protein solution was titrated to pH 4.9. Usually no correction of the pH was necessary after the protein was dissolved in the buffer. NMR samples of the reduced form of MerP were prepared in the same way after MerP had been reduced by addition of dithiothreitol.

NMR Methods. Previously recorded 2D homonuclear 500 MHz NMR data on the oxidized form of MerP (*4*) were complemented with heteronuclear 2D and 3D NMR experiments for sequential heteronuclear assignments and for NOE assignments. A Varian Unity 600 (Swedish NMR Centre, Stockholm) or a Varian Unity plus 600 (Astra Hässle, Mölndal), equipped with triple resonance pulsed field *z*-gradient probes, was used. The following spectra were acquired: 3D HNCACB (*8*), 3D HCCH-TOCSY (*9*), ^{15}N-edited 3D NOESY-HSQC (*10*), and ^{15}N/^{13}C-edited 3D NOESY-HSQC (*11*). The spectral widths and the number of points in each dimension and the number of transients are given in Table 1. In all spectra the ^{1}H transmitter frequency was centered on the water resonance (4.7 ppm), the ^{15}N channel in the middle of the amide region (120 ppm), and the ^{13}C channel in the middle of the aliphatic region (42 ppm), with the exception of the ^{15}N/^{13}C-edited 3D NOESY-HSQC spectrum where the ^{13}C channel was centered at 64 ppm. The mixing time in the NOESY experiments was 150 ms. All spectra were acquired at a temperature of 37 °C.

The same experiments were recorded on the reduced form of MerP using the same conditions as in the experiments with the oxidized form of MerP. In addition, gradient-enhanced 2D (^{1}H−^{15}N)-HSQC experiments were recorded on the reduced and the mercury-bound forms of MerP at different pH values (4.9 and 6.5). These 2D experiments were recorded on a Bruker AMX2 spectrometer operating at 500 MHz.

The spectra were processed with the CCNMR program (written by Christian Cieslar at the Max Plank Institute, Martinsried, Germany) running on a Silicon Graphics R4000 workstation. The data were processed with a Gaussian window function in t_2 and t_3 and a shifted squared sine bell window function in t_1. Zero-filling was used in the t_3 and linear prediction by 50% was used in the t_1 and t_2 dimensions prior to Fourier transformation in order to increase the resolution.

Extraction of Constraints. Interproton distance constraints were obtained from 2D NOESY, 3D ^{15}N-edited NOESY-HSQC, and 3D ^{15}N/^{13}C-edited NOESY-HSQC. The intensities of the cross-peaks were determined semiquantitatively by counting the number of contour levels of the peaks. For distances shorter than 4.0 Å, the upper bound distance was set 15% larger than the estimated distance, and for distances longer than 4.0 Å, the upper bound was set 20% larger. All lower bound distances were set to 1.9 Å.

The $^{3}J_{HN\alpha}$ coupling constants were extracted from a ^{1}H−^{15}N HMQC-J spectrum (*12*). The ψ backbone angles were extracted from $^{13}C_\alpha$ chemical shifts as described previously (*13*, *14*). Only backbone dihedral angles of the regular secondary structure elements were included in the structure calculation. The backbone angle φ was constrained to $-50 \pm 40°$ or $-125 \pm 40°$, and ψ was constrained to $-40 \pm 40°$ or $140 \pm 50°$ for regular α-helical or β-sheet structures, respectively. In addition, hydrogen bond distance constraints based on the analysis of amide proton−deuterium exchange experiments (*4*) and the derived secondary structures were added with target values of 1.8−2.3 Å for NH(*i*)−O(*j*) and 2.4−3.3 Å for N(*i*)−O(*j*).

Structure Calculations. All structure calculations were carried out using the X-PLOR 3.851 program (*15*), where 966 distance constraints [324 intraresidue, 252 sequential, 132 medium-range ($|i - j| \leq 5$), and 258 long-range ($|i - j| > 5$) NOE distance constraints], 56 hydrogen bond constraints, and 40 ϕ and 34 ψ dihedral angle constraints were used. Structure calculations were performed using an ab initio simulated annealing protocol, starting from randomly generated polypeptide chains, followed by simulated annealing and a simulated annealing refinement (*15*, *16*). No stereospecific assignment was made for any amino acid residue of MerP. Instead, NOE distances were averaged as $(\sum r^{-6})^{1/6}$ (*17*), in which no pseudo-atom corrections were needed (*18*), with the exception of methyl groups where a

Table 2: Structural Statistics of the Oxidized Form of MerP

RMSD from exptl distance constraints (Å)	0.035 ± 0.012
RMSD from exptl dihedral constraints (deg)	0.67 ± 0.14
RMSD from ideal covalent geometry	
bonds (Å)	0.0032 ± 0.000013
angles (deg)	0.62 ± 0.011
impropers (deg)	0.39 ± 0.019

0.3 Å upper bound correction was added and aromatic ring protons where a 1.0 Å upper bound correction was added. The force constants for the distance constraints were set to 50 kcal mol^{-1} $Å^{-2}$ throughout all the calculations, and the dihedral angle constraints were initially set to 5 kcal mol^{-1} rad^{-2} during the high-temperature dynamics and gradually increased to 200 kcal mol^{-1} rad^{-2} during the annealing stage. Fifty structures were calculated out of which 17 structures were selected on the basis of the criteria that the selected structure did not have any NOE distance constraint violations greater than 0.5 Å and dihedral angle constraint violations larger than 5°.

RESULTS AND DISCUSSION

The mean structure of the ensemble was calculated by superposition of the backbone atoms (N, C_α, C′) of residues 3−71. Atomic RMSD to the mean coordinates were 0.49 Å for backbone atoms and 1.05 Å for all the heavy atoms. The structural statistics are shown in Table 2. A plot of NOE distance constraints vs sequence number is presented in Figure 1a. Figure 1b shows a plot of the average RMSD values to the mean structure. Superpositions of the 17 best structures of oxidized MerP are presented in Figure 2. The global fold of the oxidized form of MerP is well defined except for the N- and C-termini. There are two regions that show slightly higher RMSD values. One of them ranges from residue 10 to residue 18, where the two cysteine residues are found. This loop points outward from the rest of the protein and is thus exposed to the solvent. Since there were only a few long-range NOE constraints observed in this region, it is not surprising that this loop should have higher RMSD values, although there is a disulfide bridge between residues 14 and 17. A second region which exhibits higher RMSD values is located between residues 48 and 53. This loop connects helix 2 and β-strand 3. The Ramachandran plot of the backbone ϕ and ψ angles for the 17 converged structures shows that 65.8% of the ϕ and ψ angles are found within the most favored region, 25.6% are found within the additionally allowed regions, and 7.0% are located within the generously allowed regions (*19*). Only 1.6% of the residues are found in disallowed regions. This indicates a good local geometry for the 17 converged structures.

Description of the Structure. A ribbon diagram representing the structure of oxidized MerP is shown in Figure 3. The secondary structure of oxidized MerP agrees well with the previously published global fold (*4*). It consists of two helices, one β-sheet, and several loops. The β-sheet contains four antiparallel β-strands: β1 (residues 3−8), β2 (residues 33−37), β3 (residues 42−47), and β4 (residues 69−71). β1 and β2 are separated by a loop region (residues 10−17) and helix 1 (residues 18−26). This loop contains the disulfide bridge between cysteine residues 14 and 17. There is a short loop (residues 38−41) between β-strands 2 and 3. β-Strands 3 and 4 are connected by helix 2 (residues 54−62). The antiparallel β-strands are arranged in the order $\beta4\beta1\beta3\beta2$. The two helices are located on top of the β-sheet.

Structure Comparison. Before any attempt to compare the structures of the oxidized, reduced, and mercury-bound forms of MerP is undertaken, it is important to evaluate whether observed differences can be explained by differences

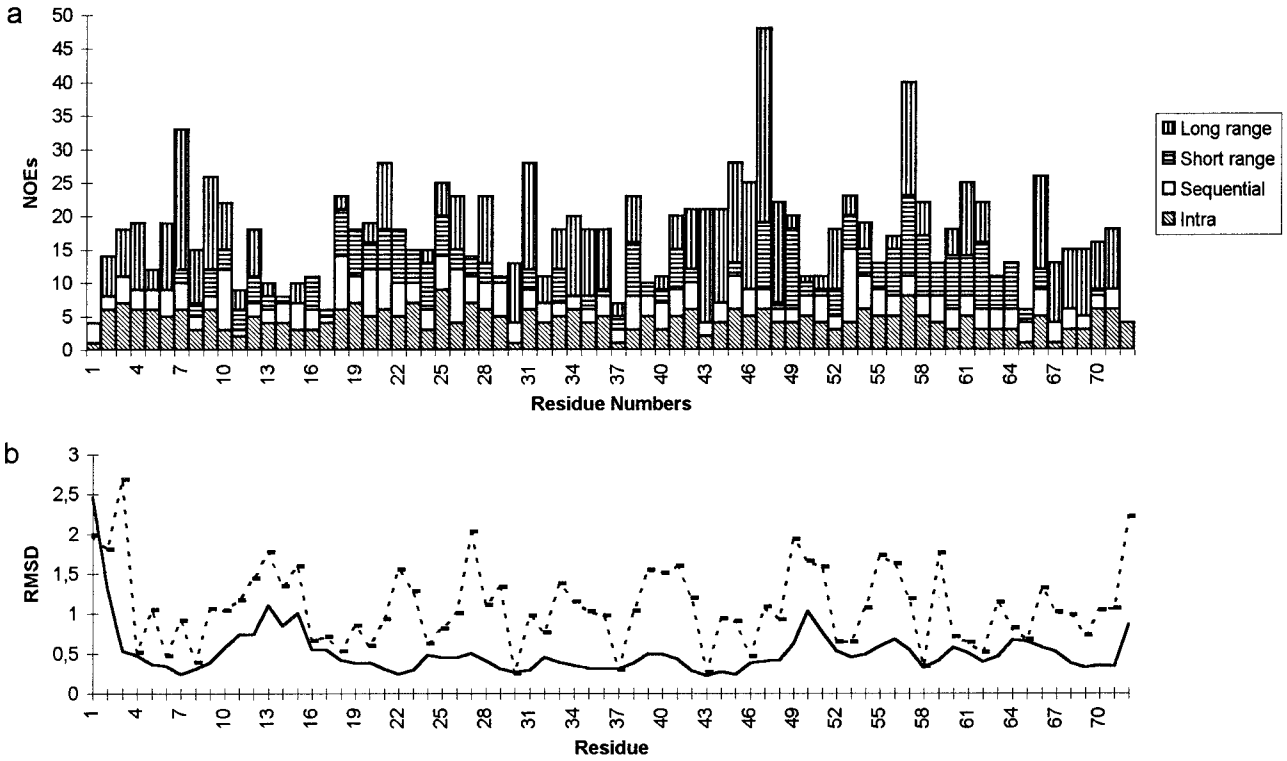

FIGURE 1: Comparison of NMR constraints and RMSD on a per residue basis. (a) Number of NOE constraints vs sequence number. (b) RMSD vs residue number for backbone atoms (solid line) and all atoms (dotted line) for the 17 best structures.

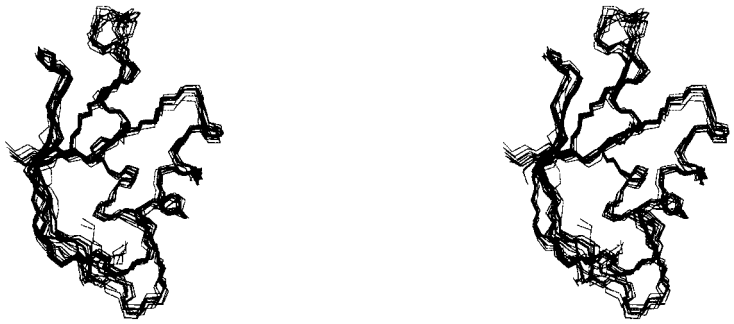

FIGURE 2: Superposition of the backbone atoms of the 17 best MerP structures.

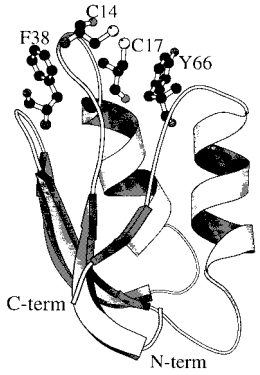

FIGURE 3: Ribbon diagram representing MerP. The two cysteine residues, 14 and 17, forming the disulfide bridge, as well as phenylalanine 38 and tyrosine 66, are highlighted.

in experimental conditions. The structure of the oxidized form presented here has been determined at pH 4.9, whereas the structures of the other two forms are based on experiments conducted at pH 6.5 (*7*). Hence, a $^{1}H-^{15}N$ HSQC spectrum of oxidized MerP at pH 6.5 was recorded to check whether the difference in pH affected the structure. This spectrum was practically identical to the spectrum acquired at pH 4.9, which demonstrates that the difference in pH does not induce any significant structural changes in oxidized MerP. Another experimental difference was that the structure of oxidized MerP was determined using the native protein, while protein used for studies of the reduced and mercury-bound forms of MerP contained an extra N-terminal sequence of five amino acids (*7*). Since no interactions could be observed between these additional amino acid residues and residues of the main protein, any perturbation of the structure of MerP from this additional peptide tail should be minor (*7*).

The program NMR-CLUST (*20*) was used to select representative structures from ensemble structures of the three different forms of MerP, oxidized, mercury-bound, and reduced (*7*), respectively. Figure 4 shows a superposition of the backbone atoms that constitute the well-defined secondary structure elements of the different forms of MerP. The global backbone RMSD difference is 2.1 Å between the oxidized and mercury-bound forms and 2.5 Å between the oxidized and the reduced forms. Figure 5 shows a plot of pairwise RMSD values vs residue numbers for the mercuric ion bound, reduced, and oxidized forms, respectively.

A few differences can be observed between oxidized, reduced, and mercury-bound MerP (*7*) at the secondary structure level. Helix 1 is formed from residues 18−28 in oxidized MerP instead of residues 17−27 for reduced MerP

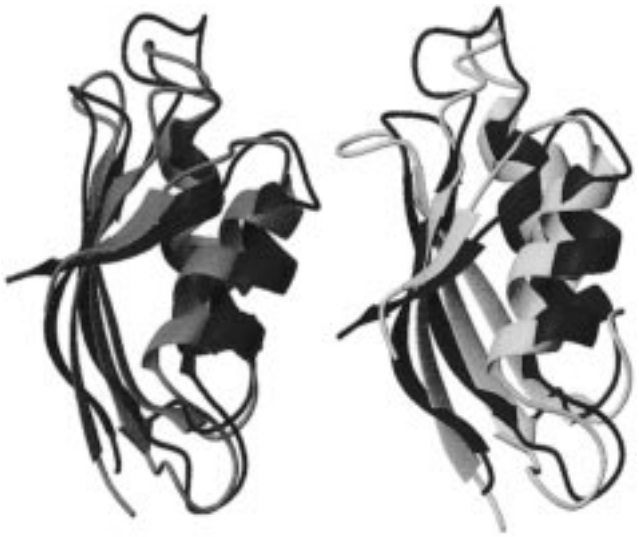

FIGURE 4: Ribbon diagrams representing oxidized MerP (in blue) superimposed on the structures of Hg^{2+}-bound MerP (a, left) and reduced MerP (b, right).

and residues 19−27 for the mercury-bound form (*7*). The major overall differences in the tertiary structure between these three different forms of MerP occur in the following regions (Figure 5): the loop between the first strand of the β-sheet and the first α-helix, where the two cysteine residues 14 and 17 are located; the loop between the second and third strands of the β-sheet comprising residues 38−41; and the region consisting of helix 2 and β-strand 4.

The differences observed between the three structures in the first loop are mainly due to the location of the cysteine residues. The loop located between residues 38−41 is close to the loop containing the two cysteines (Figure 3), so it is not surprising that there also are accompanying structural changes in this region. In both the oxidized and the Hg-bound forms, the two cysteine residues are located on the surface of the molecule, whereas in the reduced form cysteine 17 is a part of the first α-helix and not exposed to the surface. Thus, the sulfur to sulfur distances are 2.14, 4.65, and 10.02 Å for the oxidized, Hg-bound, and reduced forms, respectively. The observed movement of cysteine 17 upon reduction is in marked contrast to the behavior of the two redox-active cysteine residues in thioredoxin, another small protein where the sequence CXXC makes up the active site. In a comparison between the solution structures of reduced and oxidized thioredoxin, it was found that there were no major structural changes and the distances between the two sulfurs in the two cysteines are 2.07 and 3.82 Å for the oxidized and the reduced forms, respectively (*21*).

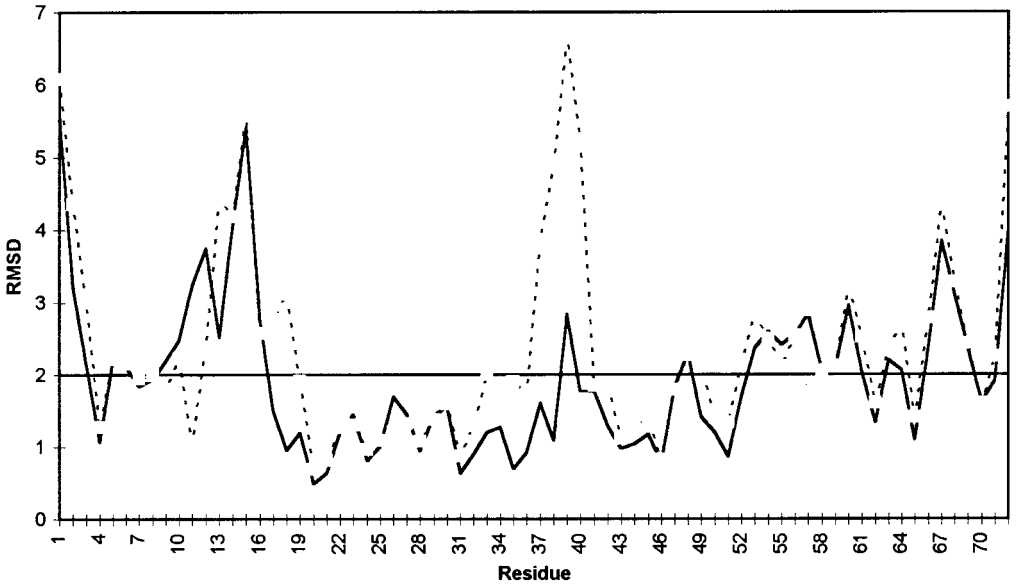

FIGURE 5: RMSD difference between oxidized MerP/mercury-bound MerP (solid line) and oxidized MerP/reduced MerP (dotted line) when the backbone atoms of all the secondary structure elements are superimposed.

Since the structural differences are largest in the cysteine-containing loop between the different forms of MerP, it is difficult to use this region as a reference point for comparison of structural differences. We have therefore superimposed all the backbone atoms of the regular secondary structure elements in the three different structures of MerP (Figures 4 and 5) in order to allow a structural comparison. The residue that experiences the most significant change in position is, of course, cysteine 17, which is radically shifted in the reduced form compared to the others. In addition, the amino acid residues in the loop located between residues 38 and 41 are also positioned differently in the reduced form. The altered location of this loop in the oxidized and Hg^{2+}-bound forms of MerP has two consequences. First, phenylalanine 38 is positioned in such a way that there is an addition of hydrophobicity that may be important for stabilizing the hydrophobic area around the cysteines in the oxidized and Hg^{2+}-bound forms. This will make the transition of the loop from the reduced conformation to the extended conformation observed in the oxidized or mercury-bound forms more favorable. This structural feature may be important in providing the right energy level required for the transition needed to bind or release mercuric ions. Second, glutamic acid 39 is also shifted considerably in the reduced form, compared to the others. Consequently, the negative charge of glutamic acid 39 is moved with respect to the mercury binding site, which may influence the way MerP binds Hg^{2+}.

The relative positions of the second α-helix and the β-sheet also contribute to the observed RMSD difference between the oxidized and the reduced or Hg^{2+}-bound forms of MerP. Despite this, the relative positions of the two helices to each other are very similar, with an interhelical angle of about 50° in all three forms of the protein. There is also a large RMSD difference for β-strand 4, which is located far apart from the first loop where the most significant differences are found.

One possibility is that the observed different positions of the region between α-helix 2 and β-strand 4 in the oxidized form and the other two forms, respectively, may be artifacts of the different approaches used in the structure calculations. The structures of the reduced and the mercury-bound forms of MerP (*7*) were based predominantly on distance constraints obtained from $^{1}H-^{15}N$ NOESY-HSQC experiments (as seen by inspection of the NOE constraint files obtained from the Protein Data Bank), whereas our structure of the oxidized form to a large extent relied on ^{13}C-edited NOESY-HSQC experiments. Thus, in the structure calculation of the oxidized form about 40−50% of the distance constraints were NOEs between aliphatic protons, and these enabled the identification of long-range NOEs for the two prolines. Hence, NOEs were observed between proline 67, located at the beginning of β-strand 4, and proline 10, located at the end of β-strand 1, as well as alanine 62, located in α-helix 2. The presence (this work) or absence (*7*) of such NOEs may affect the relative position of secondary structure elements in the calculated structures. Despite this possibility, it is likely that the observed differences reflect real structural differences, since they occur in the same regions where the amino acids undergo observable chemical shift changes upon mercuric ion titration (*7*). In addition, the differences in chemical shifts between the oxidized form and the mercury-bound form are located in the same regions and are of roughly the same magnitude. The three regions that show significant chemical shift changes upon binding to mercuric ion are the mercury binding loop and part of helix 1, the loop between residues 38 and 41, and the connecting turn between helix 2 and β4 (*7*). In summary, it is likely that the observed differences are real but it is difficult to assess the magnitude due to variations in the experimental constraints used.

Charge Distribution. The overall location of the surface charges on oxidized MerP shows a fairly large hydrophobic cluster around the active site cysteines where the disulfide bridge is exposed on the surface. This is consistent with our observation that reagents such as dithiothreitol can readily reduce the oxidized form (Powlowski and Sahlman, personal communication). The environment around the disulfide is very apolar, since there are no charged amino acids in close proximity, although the polar residue tyrosine 66 is located

on one side of the disulfide and threonine 13 on the opposite side. In contrast, the surface of MerP opposite to that encompassing the cysteine residues contains many lysines (22, 23, 27, 33, 51, 56, 59, 71). These positively charged residues are to a small extent balanced by negative charges in the form of glutamic acid 29 and aspartic acid residues 35, 48, 49, and 63. This uneven charge distribution is perhaps an explanation for the very hydrophilic reactivity of MerP during the purification, where MerP does not bind to the phenyl-Sepharose column under conditions where most proteins bind (*2*).

MerP has been proposed to function mainly as a periplasmic scavenger of Hg^{2+} (*1*, *22*). Since Hg^{2+} is positively charged, it would be repelled by positive surface charges on the surface of MerP but not by the mainly apolar area surrounding the active site cysteine residues. The positively charged surface of MerP may, on the other hand, facilitate its binding or association with negatively charged phospholipids of the membrane. Thus MerP would orient the mercuric ion binding site facing into the periplasmic space, where it would be optimized to stabilize the Hg^{2+}-bound form. This would be advantageous to the cell, since it would prevent the toxic ions from reaching other proteins in the periplasmic space or binding to the membrane itself.

Heavy-Metal Binding Motifs. There are several other proteins besides MerP where a heavy-metal binding motif, GMTCXXC, can be found in the amino acid sequence (*23*). One such example is mercuric reductase, which is an enzyme necessary for reduction of Hg^{2+} to Hg^0 in mercuric ion resistant bacteria. It contains an N-terminal region of approximately 80 amino acids which shows 30% homology to MerP. Interestingly, this domain seems to have no function in catalysis (*24*). This motif can also be found in the copper transporting proteins involved in Wilson and Menkes diseases (*23*). The Menkes' copper transporting ATPase contains six repeats of this motif in the N-terminus. The fourth one of these, mbd4, has recently been cloned and expressed as a separate protein, and its structure has been determined by NMR (*25*). As discussed by Gitschier et al., mbd4 shows structural as well as sequence similarities to MerP. Like MerP it seems to bind the metal in a bidentate complex between the sulfurs of cysteine 14 and cysteine 17. However, the big shift of cysteine 17 seen in MerP upon Hg^{2+} binding was not detected in mbd4, where the position of cysteine 17 seems to be the same regardless of whether the metal is bound or not. There is also a hydrophobic core of amino acids in both proteins as illustrated by leucine 7, valine 9, valine 21, leucine 25, valine 31, valine 36, valine 45, leucine 57, and valine 70 in MerP. There is another set of conserved hydrophobic residues, isoleucine 21, leucine 38, and phenylalanine 66 for mbd4 and phenylalanine 38 and tyrosine 66 for MerP. The functional role of these amino acids, which are located in the proximity of the metal ion binding loop, is most likely to stabilize the extended conformation of the metal ion binding loop by addition of hydrophobicity. Both proteins also contain three conserved glycines (11, 30, and 65), which all are located in the beginning of various loops. It is possible that glycine 11, which in MerP is located at the beginning of the mercuric ion binding loop, adds conformational flexibility to the binding loop and thereby facilitates binding of mercuric ions. This is analogous to the function of a conserved glycine residue in typical calcium ion binding loops (*26*). The other two glycines (residues 30 and 65) may have similar functions. Gitschier et al. (*25*) suggest that the glycines in mbd4 are necessary to allow the following amino acids to adopt a correct orientation. It was suggested that this was due to the observed positive ϕ angles, but in MerP both negative and positive values are found, suggesting that it is rather the flexibility provided by the glycines that is important than certain preferred angles.

pH-Induced Changes in the Structure. The observed different conformations of the cysteine-containing loop suggest that it is the sulfur−sulfur or sulfur−mercuric ion interactions that are mainly responsible for the stabilization of the extended conformation. However, a conformational change of this loop can also be induced in the reduced form by protonation of the thiolate anion of cysteine 17, which has a pK_a value of approximately 6 (Powlowski and Sahlman, personal communication). When the $^1H-^{15}N$ HSQC spectra of reduced MerP recorded at pH 6.5 and 4.9, respectively, were compared, large chemical shift changes could be observed which indicate that a conformational change accompanies the change of pH. Significantly, no similar conformational changes were observed for the oxidized form at these two pH values, thus suggesting that the observed pH-dependent changes in the reduced form were due to protonation of one or both of the free thiols. A qualitative analysis of the 3D ^{15}N-edited NOESY spectrum recorded on reduced MerP at pH 4.9 revealed that the mercury binding loop adopted a structure similar to the one observed in the mercury-bound or oxidized form of MerP, since all of the NOEs between cysteine 17 and phenylalanine 38 that are observable in the reduced form at pH 6.5 are absent at pH 4.9. Additional support for the notion that the reduced form at pH 4.9 has a conformation similar to that of the mercury-bound form is that only small changes (less than 0.3 ppm for both δ ^1H and δ ^{15}N) are observed when it binds mercury at this pH. This shows that in the deprotonated state the thiol group of cysteine 17 is not solvent exposed but that upon protonation the conformation is changed. The position of the thiolate anion can, in the structure of reduced MerP at pH 6.5, be stabilized by the helix dipole of the N-terminus of helix 1 as well as by the hydroxyl group of threonine 13.

Accordingly, it appears that the cysteine-containing loop can adopt at least two different conformations in the reduced form of MerP that both are energetically accessible at physiological pH. The conformation observed at lower pH is presumably stabilized by hydrophobic interactions with phenylalanine 38 and tyrosine 66, which in the structures of the oxidized and Hg^{2+}-bound forms of MerP are located close to and on opposite sides of the loop.

The presence of these different conformations may bear some resemblance with what is observed in the mbd4 domain of Menkes copper transporting ATPase. In that case the NMR resonances of serine 16 and threonine 13, located in the metal binding loop, were not observable. This was suggested to be due to conformational exchange (*25*).

CONCLUSIONS

We have presented the structure of the oxidized form of MerP. The structure agrees well with the previously published secondary structure and global fold. In addition,

the structure shows an overall agreement with the structures of the reduced and mercuric ion bound forms of MerP. In particular, the structure of the mercury-bound form of MerP is similar to that of the oxidized form, whereas the reduced form at pH 6.5 adopts a completely different conformation of the mercury binding loop where cysteine 17 is not exposed to the surface. Our data indicate that hydrophobic interactions with the aromatic residues phenylalanine 38 and tyrosine 66 could make the conformation of the loop with cysteine 17 exposed energetically accessible, since it is also possible to induce a similar conformation of the reduced form by lowering the pH. Since the pK_a value for cysteine 17 is near 6 (Powlowski and Sahlman, personal communication), at physiological pH some of the reduced form of MerP will adapt a conformation similar to what is observed in the mercury-bound form. This may be important for the affinity for mercuric ions.

Aside from the differences in the Hg^{2+} binding loop between the oxidized form and the reduced/Hg^{2+}-complexed forms, small differences are observed in the region containing the second α-helix and the last β-strand. It is difficult to predict any functional consequence of this structural difference, especially since it is not clear to what extent this structural variation reflects real structural differences or is due to differences in the experimental constraints used.

With structures of the three forms of MerP available, it is now possible to make predictions about the function of MerP, based on the structural characteristics. Thus, we conclude that the changes of the conformation of the loop consisting of residues 38−41 that occur on mercury binding or oxidation are important. With this conformation the extended cysteine-containing loop can be stabilized by hydrophobic interactions with the aromatic residues phenylalanine 38 and tyrosine 66. Another interesting feature is that the differences in function between the three different forms are related to conformational differences that only occur close to the mercury binding site. This indicates that MerP is not homologous to other periplasmic binding proteins where ligand binding induces a large conformational change. This result is in agreement with other findings from the mercuric ion resistance system, which indicate that MerP acts as a Hg^{2+} sink and not primarily as a donor in transmembrane transport (*1*).

ACKNOWLEDGMENT

We thank Justin Powlowski for useful discussions and comments on the manuscript. The Swedish NMR Center and Astra Hässle AB are acknowledged for use of their NMR instruments.

REFERENCES

1. Sahlman, L., Wong, W., and Powlowski, J. (1997) *J. Biol. Chem. 272*, 29518−29526.
2. Sahlman, L., and Jonsson, B.-H. (1992) *Eur. J. Biochem. 205*, 375−381.
3. Sahlman, L., and Skärfstad, E. G. (1993) *Biochem. Biophys. Res. Commun. 196*, 583−588.
4. Eriksson, P. O., and Sahlman, L. (1993) *J. Biomol. NMR 3*, 613−626.
5. Richardson, J. (1981) *Adv. Protein Chem. 34*, 167−339.
6. Quiocho, F. A., and Ledvina, P. S. (1996) *Mol. Microbiol. 20*, 17−25.
7. Steele, R. A., and Opella, S. J. (1997) *Biochemistry 36*, 6885−6895.
8. Muhandiram, D. R., and Kay, L. E. (1994) *J. Magn. Reson., Ser. B 103*, 203-216.
9. Kay, L. E., Xu, G.-Y., Singer, A. U., Muhandiram, D. R., and Forman-Kay, J. D. (1993) *J. Magn. Reson., Ser. B 101*, 333−337.
10. Zhang et al. (1994) *J. Biomol. NMR 4*, 845.
11. Pascal, S. M., Muhandiram, D. R., Yamazaki, T., Forman-Kay, J. D., and Kay, L. E. (1994) *J. Magn. Reson., Ser. B 103*, 197−201.
12. Kay, L. E., and Bax, A. (1990) *J. Magn. Reson. 86*, 110−126.
13. Luginbühl, P., Szyperski, T., and Wüthrich, K. (1995) *J. Magn. Reson., Ser. B 109*, 229−233.
14. Spera, S., and Bax, A. (1991) *J. Am. Chem. Soc. 113*, 5490−5492.
15. Brünger, A. T (1996) *X-PLOR Manual Version 3.843*, Yale University, New Haven, CT.
16. Nilges, M., Gronenborn, A. M., Brünger, A. T., and Clore, G. M. (1988) *Protein Eng. 2*, 27−38.
17. Nilges, M. A. (1993) *Proteins 17*, 295−309.
18. Fletcher, C. M., Jones, D. N. M., Diamond, R., and Neuhaus, D. (1996) *J. Biomol. NMR 8*, 292−310.
19. Laskowski, R. A., MacArther, M. W., Moss, D. S., and Thornton, J. M. (1993) *J. Appl. Crystallogr. 26*, 283−291.
20. Kelly, L. A., Gardner, S. P., and Sutcliffe, M. J. (1996) *Protein Eng. 9*, 1063−1065.
21. Jeng, M.-F., Campbell, A. P., Begley, T., Holmgren, A., Case, D. A., Wright, P. E., and Dyson, H. J. (1994) *Structure 2*, 853−868.
22. Summers, A. O. (1986) *Annu. Rev. Microbiol. 40*, 607−634.
23. Bull, P. C., and Cox, D. W. (1994) *Trends Genet. 10*, 246−252.
24. Fox, B. S., and Walsh, C. T. (1983) *Biochemistry 22*, 4082−4088.
25. Gitschier, J., Moffat, B., Reilly, D., Wood, W. I., and Fairbrother, W. J. (1998) *Nat. Struct. Biol. 5*, 47−54.
26. Branden, C., and Tooze, J. (1991) *Introduction to Protein Structure*, Garland Publishing Inc., New York.

BI9803628